Appl. Phys. A 67, 39–46 (1998)

Applied Physics A
Materials
Science & Processing

Theory of growth and mechanical properties of nanotubes

J. Bernholc[1], C. Brabec[1], M. Buongiorno Nardelli[1], A. Maiti[2], C. Roland[1], B.I. Yakobson[1]

[1] Department of Physics, NC State University, Raleigh, NC 27695-8202, USA
[2] Molecular Simulations, Inc., 8 N. E. Executive Park, Burlington, MA 01803-5297, USA

Received: 11 January 1998

Abstract. We have investigated the growth and mechanical properties of carbon nanotubes using a variety of complementary theoretical techniques. Ab initio molecular dynamics calculations show that the high electric field present at the tube tips in an arc-discharge apparatus is not the critical factor responsible for open-ended growth. We then show by explicit molecular dynamics simulations of nanotube growth that tubes wider than a critical diameter of ≈ 3 nm, that are initially open, can continue to grow straight and maintain an all-hexagonal structure. Narrower tubes readily nucleate curved, pentagonal structures that lead to tube closure with further addition of atoms. However, if a nanotube is forced to remain open by the presence of a metal cluster, defect-free growth can continue. For growth catalyzed by metal particles, nanometer-sized protrusions on the particle surface lead to the nucleation of very narrow tubes. Wide bumps lead to a strained graphene sheet and no nanotube growth. We have also simulated the growth and properties of double-walled nanotubes with the aim of investigating the role of lip–lip interactions on nanotube growth. Surprisingly, the lip–lip interaction by itself does not stabilize open-ended growth, but rather facilitates tube closure by mediating the transfer of atoms between inner and outer shells. Furthermore, a simulation of growth on a wide double-wall nanotube leads to considerable deviations from the ideal structure, in contrast to corresponding simulations for single-wall tubes that result in nearly perfect structures. As regards mechanical properties, carbon nanotubes, when subjected to large deformations, reversibly switch into different morphological patterns. Each shape change corresponds to an abrupt release of energy and a singularity in the stress–strain curve. The transformations, observed in molecular dynamics simulations, are explained well by a continuum shell model. With properly chosen parameters, the model provides a remarkably accurate "roadmap" of nanotube behavior beyond Hooke's law. We have also investigated static and dynamical properties of carbon nanotubes under uniaxial tension by quantum and classical simulations. In strained nanotubes at high temperatures double pentagon–heptagon defect pairs are spontaneously formed. Their formation is energetically favorable at strains greater than 5%. They act as nucleation centers for the formation of dislocations in the originally ideal graphite network and lead to the onset of a plastic deformation of the carbon nanotube.

Carbon is a rare element in its ability to form a wide variety of network-like structures, termed fullerenes. These range from the now-famous C_{60} and other large carbon cages [1] to buckyonions [2] and nanotubes [3–5]. At present, carbon nanotubes show substantial promise as superstrong fibers, composites, catalysts, molecular wires, straws, gears, switches, and photonic materials [6–15]. Success in most of the proposed applications depends crucially on the ability to synthesize coherent, defect-free nanotubes or nanotube assembly. An atomistic-level understanding of the structural, growth, defect, and elastic properties of nanotubes is, therefore, of significant technological importance.

Carbon nanotubes are currently synthesized in carbon arcs [3–5, 16, 17] through laser vaporization [18, 19], catalytic combustion [20, 21], chemical vapor deposition [22], and ion bombardment. The type of nanotube that is produced depends strongly upon the presence or absence of catalysts: multiwalled nanotubes are most commonly produced via noncatalytic means, whereas single-wall tubes are usually the dominant products under catalytic growth conditions. Given these different techniques for production, it is likely that a variety of mechanisms play a role in the assembly of nanotubes. In Sect. 1 we review our work concerning the mechanisms of growth of carbon nanotubes in the arc discharge, both single and multiwalled, with and without the presence of metal clusters, which act as catalysts. We have not yet addressed the growth assisted by highly dispersed metal atoms that occurs when a mixture of carbon and a catalyst is vaporized by a strong laser pulse.

One of the most important applications of carbon nanotubes is likely to take advantage of their outstanding mechanical properties, namely their extreme flexibility, and strength [11, 23, 24], at one-sixth the weight of steel. In Sect. 2 we review the most important aspects of the mechanical properties of nanotubes, as revealed by classical and

quantum simulations and continuum modeling. It is important to note that these results represent true predictions, since sufficiently long, defect-free nanotubes that would enable precise measurements of their strength are yet to be made. Nevertheless, the quantitative predictions are rather exciting and provide a strong impetus for further development of methods for large-scale growth of nanotubes.

1 Growth kinetics of carbon nanotubes

In this section we present the results of extensive theoretical studies of the growth of carbon nanotubes in an arc discharge, both with and without the presence of metal catalysts. Because the nanotubes form under highly nonequilibrium conditions, the kinetics of their growth is important and, as will be shown below, may even play the dominant role in a number of growth processes.

1.1 Growth from vapor phase

Initially it was believed that the tubes grow through the addition of atoms to the caps of closed tubes [25]. However, experiments show that the growth of the tubes is open-ended [5]. This is surprising, because the large number of dangling bonds at the tips of open tubes energetically favor a closed-tube geometry. A number of reasons have been suggested to explain this. Amongst these, the idea that large electric fields $\approx 1\,\mathrm{V/\AA}$ present at the tips of the growing nanotubes keep them open is quite attractive [26]. However, we have shown by ab initio calculations that even for very narrow tubes the electric field alone cannot stabilize the open-tube structure [27]. Thus, some other mechanism must be responsible. Although the idea that hydrogen atoms temporarily saturate the dangling bonds and keep the tubes open is attractive, such a mechanism is ruled out by the virtually complete exclusion of H in the arc discharge experiments. The presence of thermal or concentration gradients of large enough magnitude at the tube tips can also be ruled out. It is therefore natural to search for models based on the stability of local structures formed during growth. Therefore, we have investigated the structures that form during deposition and their subsequent dynamics.

To explore the relative stability of the various adatom structures, we first performed total-energy calculations using a many-body potential of the Tersoff form [28] with parameters from Brenner [29]. A number of all-hexagonal open tubes with varying helicities were constructed. Carbon atoms, dimers, or trimers were added to the tube tip in order to form the various possible structures occurring during growth. These structures were then relaxed by the conjugate gradient method, their energies measured and compared.

Of the various possible adatom structures that might form by the addition of atoms and small carbon clusters to the open nanotube tip, two turn out to be most important in deciding whether a tube is going to grow or close. These are a hexagon and a pair of adjacent pentagons at a "step edge", where a row of hexagons terminates at the tube tip. The adjacent pentagonal structure saturates one more dangling bonds than the hexagon, but at the same time gives rise to a curved structure at the tip. Such curved structures are energetically favored only for very narrow tubes. Our calculations show that there is a critical diameter of ≈ 3 nm, above which all-hexagonal structures with possibly a few isolated pentagons at the tube tip are energetically favored. These pentagons are converted to hexagons by the insertion of subsequent deposits and straight, defect-free growth can continue. Narrower tubes, on the other hand, favor highly curved adjacent pentagonal structures at the step edges that lead to tube closure with addition of atoms, and thus cannot grow.

The above conclusions, based on energetic arguments, have been subsequently proven by explicit molecular dynamics (MD) simulations [30]. Figure 1 illustrates the growth of a wide tube through snapshots of a specific growth simulation near a step edge on a 6.0-nm-diameter tube. In contrast, narrow tubes close through the formation of stable high-curvature pentagons [30]. Further deposition on the closed top leads to a disordered cap structure not suitable for an all-hexagonal growth. The above results help explain (a) why nanotubes grow open-ended, and (b) why, in the absence of metal catalysts, only tubes wider than ≈ 2.2 nm are observed in arc discharge.

Because of the inherent mismatch between the simulation times presently accessible to a classical MD simulation

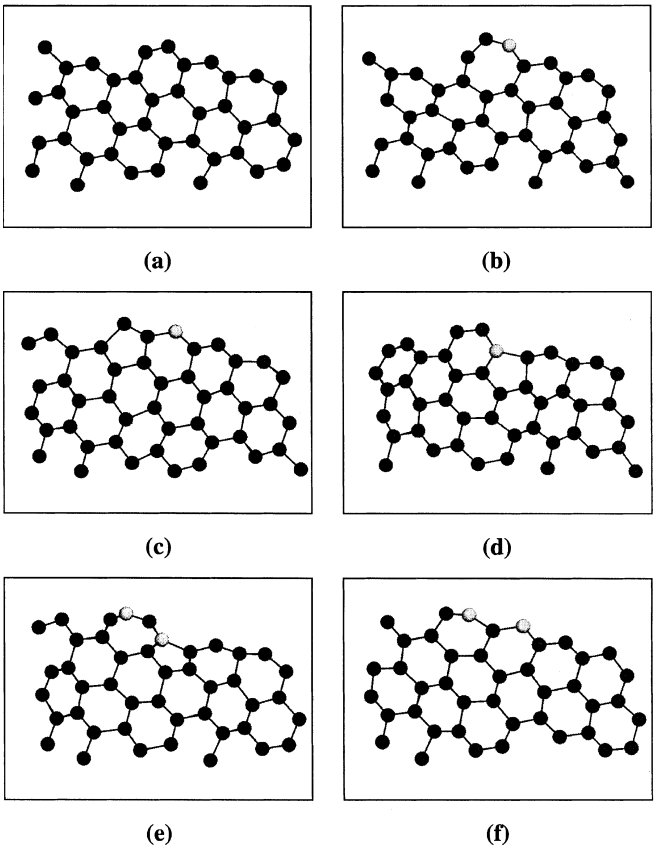

Fig. 1a–f. A specific growth simulation near a step edge on a 6.0-nm-diameter tube with helicity (59,27). **a** The initial all-hexagonal structure remains stable upon annealing even at our high simulation temperature of 3000 K. **b** The first atom inserts itself to form a heptagon at the step edge, which **c** quickly decomposes into a hexagon and a pentagon at the step edge. **d** The pentagon then swaps with the adjacent hexagon through a bond switch and migrates by one ring. **e** A second deposited atom inserts into the hexagon at the step edge to form a heptagon, which **f** then annihilates with the migrating pentagon to form an open-ended, all hexagonal structure

(nanoseconds) and the long experimental growth times (milliseconds), it is not possible to simulate large-scale growth of carbon nanotubes directly, without assuming unrealistically large deposition rates. In order to reach experimental timescales, we incorporated information on basic bond-switching kinetics obtained from the MD simulations into a kinetic Monte Carlo code [31]. In addition to allowing growth simulations to be performed over experimental times, the Monte Carlo code also estimated a minimum temperature of ≈ 1000 K required for defect-free growth, in good agreement with experimental observations.

1.2 Growth in the presence of metal catalysts

The first syntheses of single-walled graphitic tubes (SWTs) in the presence of metal catalysts [16, 17] and the recently discovered laser-vaporization method of making nanotubes in significantly larger quantities [19] have instilled a new impetus into the study of their growth. SWTs are expected to be much freer of defects than the multiwalled nanotubes synthesized previously. Not surprisingly, therefore, intense activities among many research groups have yielded successful synthesis of SWTs using many different catalysts; transition metals Fe, Co, Ni, and Cu; lanthanide metals Gd, Y, and La, as well as several mixed catalysts [32–37]. Nanotubes produced in these experiments show a relatively narrow dispersion in diameter, varying between 0.8 and 3.1 nm depending on the catalyst used, and the longest tubes grow up to a few μm. Metal-catalytic growth of these nanotubes is widely believed to proceed via solvation of carbon vapor into metal clusters, followed by precipitation of excess carbon in the form of nanotubes. In the laser-vaporization experiments, on the other hand, the growth is believed to be catalyzed by single metal atoms [19, 38]. In this subsection, we will only discuss the growth catalyzed by metal particles, or clusters.

Depending on the size of the clusters involved, there are two different modes of catalytic growth of SWTs; (mode 1) in which the metal particles, several tens of nm wide, are much larger than the tube diameters and lead to the precipitation of a large number of SWTs from a single particle surface [32, 34], and (mode 2) in which the metal particles are of the same size or even smaller than the tube diameters (≈ 1 nm) and prevent tube closure by moving with the growing tip [37]. SWT growth by mode 2, when it occurs, is relatively simple, and is explained by the presence of reactive dangling bonds at the tube tip [31, 37]. The dangling bonds are stabilized by the metal particles and act as attraction sites for carbon adatoms.

However, mode 1, which implies root growth by carbon atoms precipitating from large metal particles, occurs in many experiments where web-like material, consisting of rounded soot particles, several tens of nm in size, forms [17]. The soot particles have been identified as metal clusters embedded in a few layers of graphitic carbon, which are interconnected by SWTs, several μm in length. Another direct evidence in support of root growth is that the use of lanthanide series catalysts (Gd, Yi, and La) yields sea urchin morphology [32–34] in which a dense bundle of SWTs emanates radially from each metal particle. The main challenges associated with growth mode 1 are to understand (i) what limits the width of all SWTs to within ≈ 3 nm, while precipitating from a metal carbide particle of size several tens of nm; and (ii) what prevents the formation of multishelled tubes.

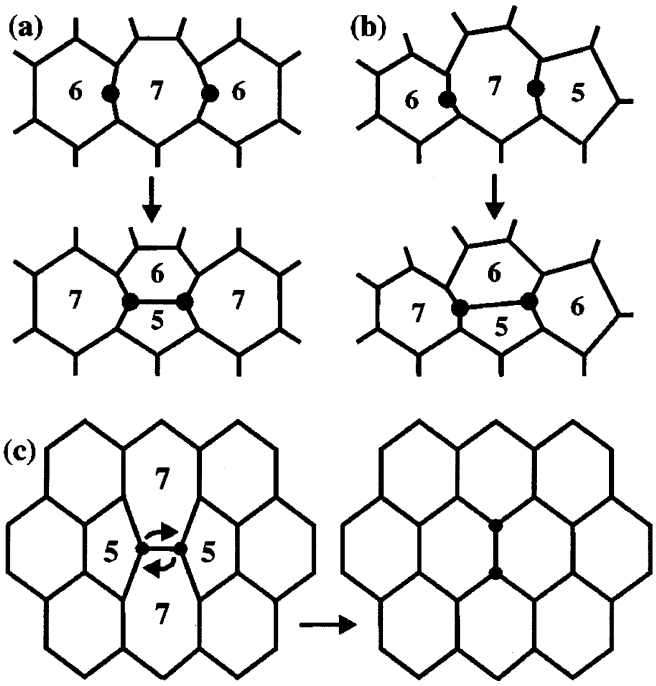

Fig. 2a–c. The atomistics of hexagon addition at the nanotube base by bond formation between a pair of handle atoms at the opposite sides of a heptagon. **a** For an isolated heptagon, a 5-7 pair forms in addition to a hexagon. **b** For a 5-7-6 complex only an additional hexagon forms. **c** Annihilation of two adjacent 5-7 pairs into four hexagons by a reverse Stone–Wales switch

We have performed extensive MD simulations to address the above points [39]. The simulations have revealed the basic atomic processes by which root growth of SWTs can occur from a metal carbide surface. We find that carbon adatoms on a graphite plane form two bonds with the "substrate" and are quite mobile. Assuming that a tube base has already formed, these "handles" are energetically attracted to it and the tube can grow. An even number of handles leads to an increase in the net number of hexagons, and thus to root growth. Through snapshots from our MD simulations, Fig. 2 illustrates the various ways in which hexagons may form at the tube base. Under the assumption that the metal surface contains protrusions of height $h \sim$ a few nm, the simulations yield the following picture: protrusions much narrower than h can nucleate and grow SWTs, whereas wider ones form only a strained graphene sheet and do not lead to tube growth. Thus, our results explain why only very narrow SWTs are observed experimentally and why multishelled tubes growing out of metal particles are usually not found.

1.3 Growth of multishell nanotubes: relevance of lip–lip interaction

We have studied the growth of multiwalled carbon nanotubes as formed in an arc discharge, with a primary focus on the so-called lip–lip interaction between adjacent tube tips [37]. Such an interaction arises when atoms or small clusters from the vapor deposit themselves at the tips of the nanotubes. These then form bridges or "spot-welds" between the tubes, which are thereby kept open for continued growth.

To investigate the importance of the lip–lip interactions, we have carried out extensive molecular dynamics (MD) simulations of double-walled carbon nanotubes [40]. We first constructed a (10,0)@(18,0) multiwalled tube having a height of 12 atomic layers [41], which was then uniformly heated up from 0 to 3000 K over a 40-ps period of time. Although there was no initial interaction between the tube tips, bridging bonds were first observed to form at ≈ 900 K, when the amplitudes of the radial distortions were large enough to bring the carbon atoms of the tips within interaction range. Such bonds continued to form as the temperature was increased, until a complete network of bridging bonds was formed, as shown in Fig. 2a. The bonds of this lip–lip interaction are of a fluctuating character: on a timescale of several ps, the bonds bridging the tube tips were observed to break and reform in similar configurations. These results are in complete agreement with similar simulations based on the more accurate ab initio methods [41]. To test the efficacy of the lip–lip interaction in keeping multiwalled tubes open, we continued annealing the (10,0)@(18,0) tube. Surprisingly, we find that the double-walled tube closes spontaneously on hundreds of picoseconds timescale. The lip–lip interaction by itself simply cannot keep narrow, multiwalled tubes open for growth.

Details of a simulation of a (18,0)@(26,0) double-wall tube are shown in Fig. 3. Because of the fluctuating nature of the lip–lip interaction, bonds that bind atoms of the lip–lip network break, leading to the transfer of atoms to the inner tube. Within a timescale of ps, the lip–lip interaction reforms near those spots, but now the lips of the outer tubes are curved as compared to its initial state, as shown in the side views in Fig. 4a,b. At the same time, curvature-inducing defects, such as adjacent pentagons, readily form on the inner tube, so that it begins to curve inwards. This, of course, bends the outer tube even more, further enhancing the transfer of atoms from the outer towards the inner tube via the lip–lip network. As this network of atoms moves across the tubes, there is a general collapse of the upper parts of the inner tubes, forming a separate shell now covering only the inner tube. These observations suggest that the driving force for tube closure is set by the curvature (diameter) of the inner tube, where the defects leading to closure first form.

To compare the stability of single- and double-walled tubes, we carried out annealing studies for tubes in the ≈ 2-nm range, which are summarized in Table 1. Essentially, at any given temperature, the time required to close the double-walled tube is slightly longer than, but still comparable to, the time needed to close the single-walled tube having the same diameter as the inner double-walled tube. The closure time for the double-walled tubes is longer, simply because it takes some time for atoms to transfer from the outer to the inner tube.

While these simulations show that the lip–lip interaction alone cannot stabilize open-ended nanotubes, it is still possible that these interactions exert a stabilizing influence if they act in conjunction with other effects, such as with a large

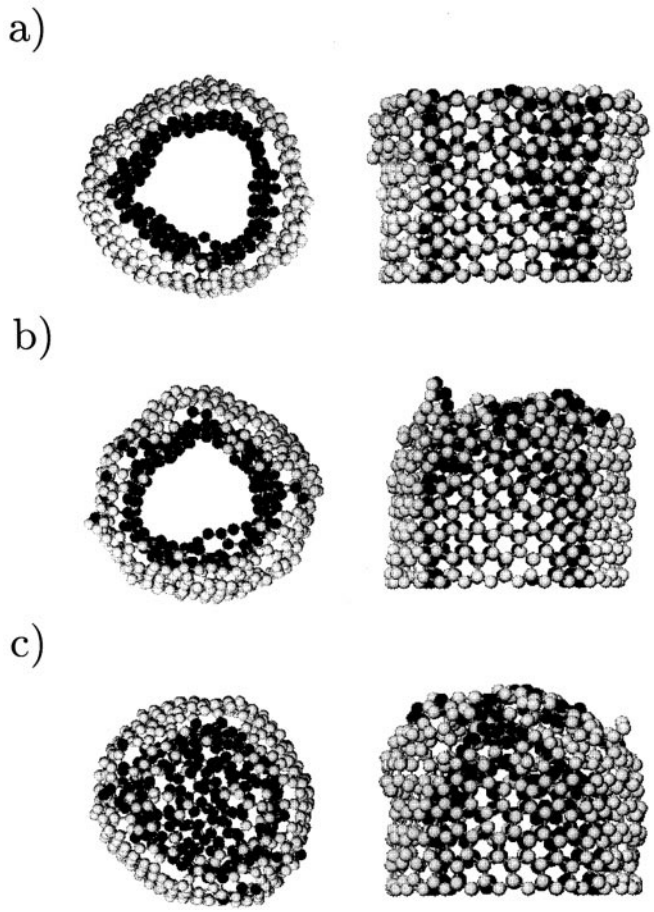

Fig. 3a–c. Top and side views of (18,0)@(26,0) double-walled tubes. Lighter (darker) colors are used to represent atoms from the outer (inner) tube. **a** 0 ps. **b** 45 ps. **c** 180 ps. Note that at these high temperatures a small number of atoms from the inner tube move towards the outer tube

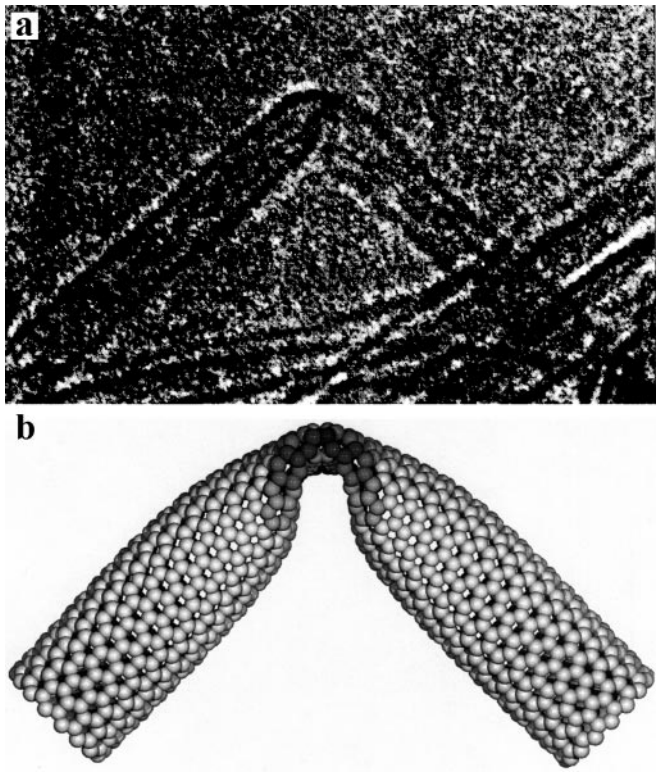

Fig. 4. a High-resolution transmission electron microscope image of a bent tube. **b** A computer-generated image of a bent tube. The network of hexagons is not disturbed; consequently, the tube can unbend without any damage

Table 1. Mean time for closure t for a series of annealing runs for single- and double-walled tubes

Tubes	Diameter /nm	Temperature /K	t /ps
(10,0)	0.78	3500	7
(10,0)	0.78	3000	45
(18,0)	1.41	3000	650
(10,0)@(18,0)		3000	154
(13,0)	1.02	3400	48
(21,0)	1.64	3400	250
(13,0)@(21,0)		3400	64
(18,0)	1.41	3500	140
(26,0)	2.03	3500	212
(18,0)@(26,0)		3500	180

electric field present at the tube tips [37]. To address this issue, we have carried out an extensive simulation of growth on a large-diameter double-walled tube, which should be relatively stable. Two saw-toothed (38,0)@(47,0) tubes having diameters of 3.0 and 3.7 nm and heights of 12 atomic layers were constructed. To form the lip–lip interaction, 38 atoms were added between the nanotube tips, and the system was annealed for a short period of time. During the MD run, the temperature of the tips was kept at 3000 K. A constant temperature gradient was imposed along the length of the tube, so that bottom layers were kept at 1700 K. Carbon atoms were then deposited at random around the circumference of the tube, with kinetic energies in the 1–8 eV range. The primary effect of the electric field was assumed to simply focus the incoming atoms onto the nanotube tips. As with the narrow tubes, atoms were readily incorporated into the lips of tube. However, most of the incorporation took place either on top of the lips, or at the "bends", where the curvature is the highest. This however did not lead to open-ended and straight growth. Rather disordered, cap-like "ballooning" structures were formed with considerable deviations from straight growth. Whether such disordered growth would simply continue or mark the beginning of the tube closure is at present impossible to tell.

2 Elastic and deformation properties

The remarkable flexibility of the hexagonal network allows the system to sustain very high bending angles, kinks, and highly strained regions. In addition, nanotubes are observed to be extremely resilient, suggesting that even largely distorted configurations (axially compressed, twisted) can be the result of elastic deformations with no atomic defects involved [11, 23, 42, 43]. Such a suggestion is provocative for a graphite-like material, commonly perceived as rather brittle and poses important questions: what range of strain can nanotubes sustain elastically, and what kind of patterns can they exhibit under different mechanical load? We have carried out MD studies for nanotubes under generic modes of deformation [11, 23]: bending, axial compression, and torsion. Originally the goal was to reproduce, if possible, the HRTEM "signature" of the bent nanotubes. The agreement was very good, see Fig. 4 [23]. We further found a remarkable synergism between the methods of MD and those of macroscopic structural mechanics [11]. A singular behavior of the buckytube energy at certain levels of strain corresponds to abrupt changes in morphology, when a switch between distinct patterns occurs. These transformations can be interpreted in terms of a continuous tubule with properly chosen parameters, which provides an analytical model for buckytube behavior not only at small deformations but also beyond the linear response. The energy of a shell is given by a surface integral of the quadratic form of local deformation [44],

$$E = \frac{1}{2}\iint \Big\{ D\left[(\kappa_x+\kappa_y)^2 - 2(1-\nu)(\kappa_x\kappa_y-\kappa_{xy}^2)\right] + \frac{C}{\left(1-\nu^2\right)}\left[(\varepsilon_x+\varepsilon_y)^2 - 2(1-\nu)\left(\varepsilon_x\varepsilon_y-\varepsilon_{xy}^2\right)\right]\Big\}\,\mathrm{d}S\,,$$

where κ is the curvature variation, ε is the in-plane strain, and x and y are local coordinates. In order to adapt this formalism to a graphitic tubule, the values $C = 59\,\mathrm{eV/atom} = 360\,\mathrm{J/m^2}$ and $D = 0.85$ eV have been identified by comparison with the MD studies of buckytube energetics at small strains.

Figure 5 shows a simulated buckytube exposed to axial compression [11]. At small strains the total energy grows as $E(\varepsilon) = 1/2C\varepsilon^2$. The presence of four singularities at higher strains is quite a striking feature and the patterns illustrate the corresponding morphological changes. The shading indicates strain energy per atom, equally spaced from below 0.5 eV (brightest) to above 1.5 eV (darkest). The sequence of singularities in $E(\varepsilon)$ corresponds to a loss of molecular symmetry from $D_{\infty h}$ to S_4, D_{2h}, C_{2h}, and C_1. This evolution is in accordance with the continuum elasticity shell model, which further allowed a derivation of simple equations describing instabilities in SWNT in different elastic deformations. These can be briefly summarized as follows. Under axial compression, the tube either buckles sideways at $\varepsilon_c' = 1/2(\pi d/L)^2$, or forms a local wall-kinks at the strain level $\varepsilon_c'' = 0.077\,\mathrm{nm\,d^{-1}}$ (whatever occurs first). Understandably, a pure sideways buckling leads further to a local bending

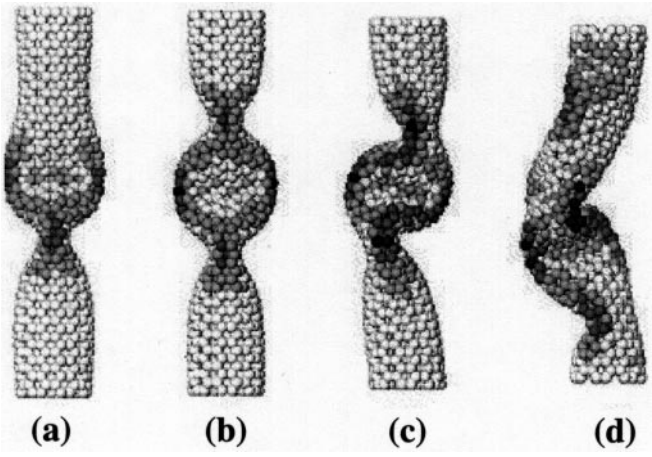

Fig. 5a–d. An MD-simulated buckytube of length $L = 6$ nm, diameter $d = 1$ nm, and armchair helicity (7,7), under axial compression. At $\varepsilon_1 = 0.05$ the cylinder buckles into a pattern (**a**), displaying two identical flattenings– "fins" perpendicular to each other. Further increase of ε enhances this pattern gradually until at $\varepsilon_2 = 0.076$ the tube switches to a three-fin pattern (**b**), still possessing a straight axis. In a buckling sideways at $\varepsilon_3 = 0.09$ the flattenings serve as hinges, and only a plane of symmetry is preserved, (**c**). At $\varepsilon_4 = 0.13$ an entirely squashed asymmetric configuration forms (**d**)

(which is the softest and more frequently observed mode of deformation). In bending, only one side of a tube is compressed and thus can buckle, and the estimated critical curvature is $K_c = 0.155\,\mathrm{nm\,d^{-2}}$. This is in excellent agreement (within 4%) with extensive simulations of single-wall tubes of various diameters, helicities, and lengths. Due to the end effects, the average curvature is less than the local one and the simulated segment buckles somewhat earlier than at $\theta_c = K_c L$, which is accurate for longer tubes.

In simulation of torsion, the increase of azimuthal angle ϕ between the tube ends results in either overall beam-buckling at $\phi'_c \approx 2\pi$, or in a cylinder-helix flattening, at $\phi''_c = 0.055\ \mathrm{nm^{3/2}L\,d^{-5/2}}$. Such flattened-collapsed structures have been observed experimentally and are caused by a combination of externally applied twist and the van der Waals attraction between the walls.

The ability of nanotubes to reversibly collapse under large hydrostatic compression is due to their hollow structure and the resilience of the graphene walls. Collapse cannot occur simultaneously throughout the tube of substantial length. It is initiated locally (for example, by a bend or twist) and then propagates with the speed ν proportional to the square root of over-pressure [45], $\nu \approx (p/p_0 - 1)^{1/2}$.This is of interest in relation to potential applications of nanotubes in shock-absorbing materials and the existing experimental evidence of such reversible collapse [46].

With the abundant evidence of high resilience of CNT in different deformations [47], it is important to assess the limits of their strength in fast-strain test simulation [48]. Nanotube behavior at high tensile strain rate ($\approx 1\,\mathrm{MHz}$) has been studied by molecular dynamics using the Tersoff–Brenner potential. The simulations performed for single- and double-walled nanotubes of different helicities and at different temperatures show that nanotubes have an extremely large ($> 25\%$) fast-breaking strain. At the breaking strain level, one or a few C−C bonds fail almost simultaneously, and the resulting "hole" in a tube wall becomes a precursor of fracture. The atomic disorder propagates then rapidly along the circumference of the tube. The strain, which was quite uniform along the tube before this threshold, redistributes itself to form a largely distorted and unstable neck between the two quickly relaxing segments of the nanotube. A further stage of fracture displays an interesting feature, the formation of two or more distinct chains of atoms, spanning the two tube fragments. Eventually, the switching of C−C bonds leads to merging of the chains and to a survival of one chain only. Remarkably, a further increase of the distance between the tube ends does not break this chain. It elongates not by virtue of straining the constituent bonds, but rather by increasing the number of carbon atoms that pop out from both sides into the necklace. This single monoatomic chain continues to grow as long as the separation between the nanotube ends increases. The level of strain within the chain remains approximately constant, and is apparently determined by the threshold force for the next atom to pop out. Although this process should have some activation energy, we did not notice a temperature dependence of the force on the ends and/or the intrachain strain. Such dependence may become detectable at a very low rate of pulling, which we did not reach in those simulations. Overall, the pulling of a monoatomic chain resembles very much the unraveling by the electric field, suggested in experimental studies [10]. In our simulations, the unraveling does not proceed in a nice simple fashion, along the edge of an open-ended nanotube, as in [10], since the dangling bonds along such edge are very unstable and tend to rebond. This complicates the unraveling, but we did see a relatively large opening, a polygon fluctuating in the size range of 7–13 vertices.

We have also investigated the strain release mechanisms under fixed-strain conditions, which at molecular dynamics time scales provides a closer approximation to the actual conditions of mechanical-load-induced failure. Under these conditions, beyond a critical value of the tension, the system releases its excess strain via a spontaneous formation of topological defects. The first defect to form corresponds to a 90° rotation of a C−C bond about its center, the so-called Stone–Wales transformation [49], which produces two pentagons and two heptagons coupled in pairs (5-7-7-5), as shown by ab initio real-space multigrid calculations [50] see Fig. 6. This topological change is stable during the remaining simulation time ($\approx 1\,\mathrm{ps}$). The energetics of this defect have been investigated via zero-temperature calculations. Both the equilibrium and the 10%-strained tubes are (meta-)stable in the ideal graphite structure and in the presence of the (5-7-7-5) defect. At zero strain, the energy of the defect configuration

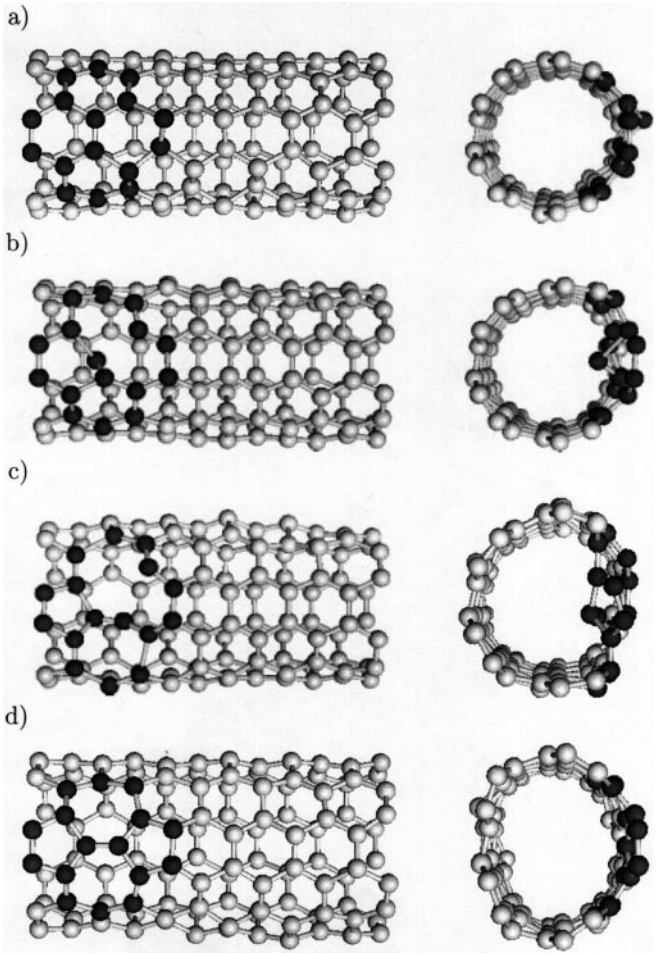

Fig. 6a–c. Kinetic mechanism of (5-7-7-5) defect formation from an ab initio quantum molecular dynamics simulation for the (5,5) tube at 1800 K. The atoms that take part in the Stone–Wales transformation are highlighted in black. The three snapshots show the various stages of the defect formation: **a** system in the ideal configurations ($t = 0.00\,\mathrm{ps}$): **b** breaking of the first bond ($t = 0.10\,\mathrm{ps}$): **c** the defect is formed ($t = 0.20\,\mathrm{ps}$)

is higher than the ideal one by 2.34 eV. However, in the 10%-strained tube, the energy of the structure with the defect is lower than the ideal one by -1.77 eV. This is because the two heptagons can be stretched more than the hexagons while keeping a C−C bond length that is close to the ideal one.

Static calculations under fixed dilation show a crossover in the stability of this defect configuration with respect to the ideal hexagonal network. This implies that the (5-7-7-5) defect is effective in releasing the excess strain energy in a tube under tensile strain. Classical potential calculations of the formation energy of a single (5-7-7-5) defect as a function of uniaxial strain have been carried out for a number of armchair tubes and for a single sheet of graphite (graphene). The defect structure starts to be energetically favored after about 5% tensile strain in the tubes and somewhat later in graphene, due to the absence of the additional strain induced by the curvature of the tubular structure. Activation energies for the bond rotation process range between ≈ 6 and 2 eV going from 0 to 20% tensile strain. As expected, the potential energy barrier decreases with the strain.

A better understanding of the kinetics of deformation of a carbon nanotube under tensile strain conditions can be gleaned from long-time classical molecular dynamics simulations on larger tubes. For this reason, we studied the time evolution of a relatively long fragment (3 nm, 480 atoms) of a (10,10) tube at 2000 K under 10% axial strain. After an initial annealing to 2000 K, with a rate of temperature increase of 50 K per ps, the system was evolved for 2.5 ns. Within the first 1.1 ns a few (5-7-7-5) defects are formed in the tube and each of them remains localized in the region where they have been formed. After 1.5 ns another (5-7-7-5) defect is formed (see Fig. 7a), which shows a peculiar time evolution. After 100 ps from its formation, the two pentagon-heptagon pairs split, and eventually one of them starts diffusing within the helical structure of the tube (Fig. 7b), while the other remains trapped in the original position by an additional (5-7-7-5) defect. After another 350 ps, the 5-7 defect that migrated from its original position transforms into another topological defect: a (5-7-5-8-5), i.e., an octagon and a pair of pentagons are added to the original pentagon–heptagon pair (Fig. 7c). From a topological point of view, the splitting of the (5-7-7-5) defect produces a remarkable effect [24, 51]: the separation and glide of 5-7 dislocations changes the chirality of the nanotube and leads to the formation of nanotube heterojunctions, as well as to the onset of possible plastic behavior in nanotubes.

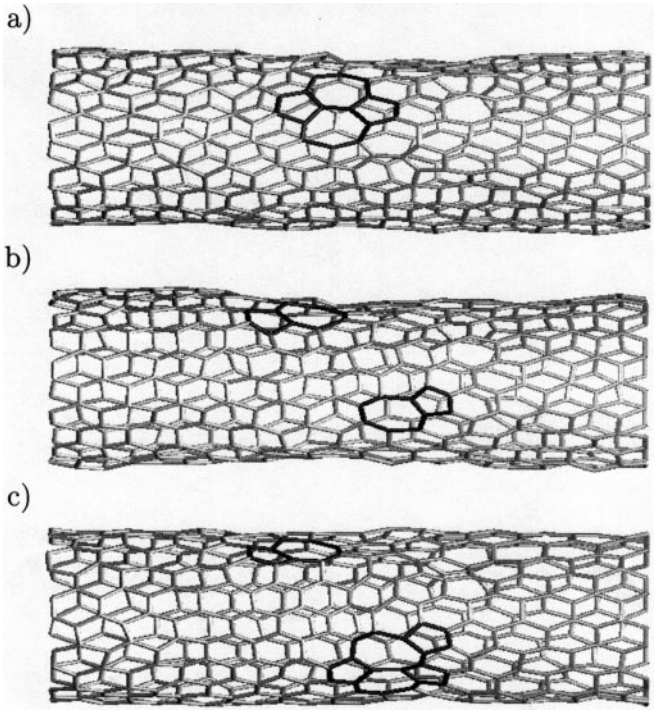

Fig. 7a–c. Time evolution of a particular (5-7-7-5) defect from a classical simulation for a (10,10) carbon nanotube at 2000 K under 10% uniaxial strain. The defect structure is highlighted in black. **a** Formation of the pentagon–heptagon defect whose evolution in time we will be followed ($t = 1.5$ ns). **b** The defect splits and starts diffusing ($t = 1.6$ ns). **c** Another bond rotation has led to the formation of a (5-7-5-8-5) defect ($t = 2.3$ ns)

References

1. H.W. Kroto, J.R. Heath, S.C. O'Brien, R.F. Curl, R.E. Smalley: Nature **318**, 162 (1985); W. Kratschmer, L.D. Lamb, K. Fostiropoulos, D.R. Huffmann: Nature **347**, 354 (1991); R. Ettl, I. Chao, F. Diederich, R.L. Whetten: Nature **353**, 149 (1991); F. Diederich, R. Ettl, Y. Rubin, R.L. Whetten, R. Beck, M. Alvarez, S. Anz, D. Sensharma, F. Wudl, K.C. Khemani, A. Koch: Science **252**, 548 (1991); K. Kikuchi, N. Nakahara, T. Wakabyashi, S. Suzuki, H. Shimomaru, Y. Miyake, K. Saito, I. Ikemoto, M. Kainosho, Y. Achiba: Nature **357**, 142 (1992)
2. D. Ugarte: Nature **359**, 707 (1992); Europhys. Lett. **22**, 45 (1993)
3. S. Iijima: Nature **354**, 56 (1991)
4. T.W. Ebbesen, P.M. Ajajan: Nature **358**, 220 (1992)
5. S. Iijima, P.M. Ajajan, I. Ichihashi: Phys. Rev. Lett. **69**, 3100 (1992)
6. P. Calvert: Nature **357**, 365 (1992)
7. P. Ross: Sci. Am. **264**(6), 16 (1991)
8. J. Broughton, M. Pederson: Phys. Rev. Lett. **69**, 2689 (1992)
9. D.T. Colbert, J. Zhang, S.M. McClure, P. Nikolaev, Z. Chen, J.H. Hafner, D.W. Owens, P.G. Kotula, C.G. Carter, J.H. Weaver, A.G. Rinzler, R.E. Smalley: Science **266**, 1218 (1994)
10. A.G. Rinzler, J.B. Haffner, P. Nikolaev, L. Lou, S.G. Kim, D. Tomanek, P. Nordlander, D.T. Colbert, R.E. Smalley: Science **269**, 1550 (1995)
11. B.I. Yakobson, C. Brabec, J. Bernholc: Phys. Rev. Lett. **76**, 2511 (1996)
12. See, for example, M.S. Dresselhaus, G. Dresselhaus, P.C. Eklund: *The Science of Fullerenes and Carbon Nanotubes* (Academic Press, San Diego 1996)
13. F.J. Garcia-Vidal, J.M. Pitarke, J.B. Pendry: Phys. Rev. Lett. **78**, 4289 (1997)
14. J. Han, A. Globus, R. Jaffe, G. Deardorff: Nanotechnology **8**, 95 (1997)
15. M. Menon, D. Srivastava: Phys. Rev. Lett. **79**, 4453 (1997)
16. S. Iijima, T. Ichihashi: Nature **363**, 603 (1993)
17. D.S. Bethune, C.H. Kiang, M.S. deVries, G. Gorman, R. Savoy, J. Vazquez, R. Beyers: Nature **363**, 605 (1993)
18. T. Guo, D. Nikolaev, A.G. Rinzler, D. Tomanek, D.T. Colbert, R.E. Smalley: J. Chem. Phys. **99**, 10694 (1995)
19. A. Thess, R. Lee, P. Nikolaev, H. Dai, P. Petit, J. Robert, C. Xu, Y.H. Lee, S.G. Kim, A.G. Rinzler, D.T. Colbert, G.E. Scuseria, D. Tomanek, J.E. Fisher, R.E. Smalley: Science **273**, 483 (1996)
20. H. Hatta, K. Murata: Chem. Phys. Lett. **217**, 398 (1994)
21. H. Dai, A.G. Rinzler, P. Nikolaev, A. Thess, D.T. Colbert, R.E. Smalley: Chem. Phys. Lett. **260**, 471 (1996)
22. W.Z. Li, S.S. Xie, L.X. Qian, B.H. Chang, B.S. Zou, W.Y. Zhou, R.A. Zhao, G. Wang: Science **274**, 1701 (1996)
23. S. Iijima, C. Brabec, A. Maiti, J. Bernholc: J. Chem. Phys. **104**, 2089 (1996)
24. M. Buongiorno Nardelli, B.I. Yakobson, J. Bernholc: Phys. Rev. B **57**, R4277 (1998)
25. M. Endo, H.W. Kroto: J. Phys. Chem., **96**, 6941 (1992); R. Saito, G. Dresselhaus, M.S. Dresselhaus: Chem. Phys. Lett. **195**, 537 (1992)
26. R. Smalley: Mater. Sci. Eng. B **19**, 1 (1993)
27. A. Maiti, C. Brabec, C. Roland, J. Bernholc: Phys. Rev. Lett. **73**, 2468 (1994)

28. J. Tersoff: Phys. Rev. Lett. **56**, 632 (1986); *ibid* **61**, 2879 (1988); Phys. Rev. B **37**, 6991 (1988)
29. D.W. Brenner: Phys. Rev. B **42**, 9458 (1990)
30. C.J. Brabec, A. Maiti, C. Roland, J. Bernholc: Chem. Phys. Lett. **236**, 150 (1995)
31. A. Maiti, C.J. Brabec, C. Roland, J. Bernholc: Phys. Rev. B **52**, 14850 (1995)
32. Y. Saito, T. Yoshikawa, M. Okuda, M. Fujimoto, K. Symiyama, K. Suzuki, A. Kasuya, Y. Nishina: J. Phys. Chem. Sol. **54**, 1849 (1993); Y. Saito, M. Okuda, N. Fujimoto, T. Yoshikawa, M. Tomita, T. Hayashi: Jpn. J. Appl. Phys. **33**, L-526 (1994); Y. Saito: In *Recent Advances in the Chemistry and Physics of Fullerenes and Related Materials*, ed. by K.M. Kadish, R.S. Ruoff (ECS, Pennington 1994) p. 1419; Y. Saito, M. Okuda, M. Tomita, T. Hayashi: Chem. Phys. Lett. **236**, 419 (1995)
33. S. Subramoney, R.S. Ruoff, D.C. Lorents, R. Malhotra: Nature **366**, 637 (1993)
34. S. Seraphin, D. Zhou: Appl. Phys. Lett. **64**, 2087 (1994); D. Zhou, S. Seraphin, S. Wang: Appl. Phys. Lett. **65**, 1593 (1994)
35. X. Lin, X.K. Wang, V.P. Dravid, R.P.H. Chang, J.B. Ketterson: Appl. Phys. Lett. **64**, 181 (1994)
36. J.M. Lambert, P.M. Ajayan, P. Bernier, J.M. Planeix, V. Brotons, B. Coq, J. Castaing: Chem. Phys. Lett. **226**, 364 (1994)
37. T. Guo, P. Nikolaev, A. Thess, D.T. Colbert, R.E. Smalley: Chem. Phys. Lett. **243**, 49 (1995)
38. L. Young Hee, K. Seong Gon, D. Tomanek: Phys. Rev. Lett. **78**, 2393 (1997)
39. A. Maiti, C.J. Brabec, J. Bernholc: Phys. Rev. B **55**, R6097 (1997)
40. M. Buongiorno Nardelli, C.J. Brabec, A. Maiti, C. Roland, J. Bernholc: Phys. Rev. Lett. **80**, 313 (1998)
41. J.C. Charlier, A. DeVita, X. Blase, R. Car: Science **275**, 646 (1997)
42. J. Despres, E. Daguerre, K. Lafdi: Carbon **33**, 87 (1995)
43. N. Chopra, L. Benedict, V. Crespi, M.L. Cohen, S.G. Louie, A. Zettl: Nature **377**, 135 (1995); R. Ruoff, D. Lorents: Bull. Am. Phys. Soc. **40**, 173 (1995)
44. S.A. Safran: *Statistical Thermodynamics of Surfaces, Interfaces and Membranes*, Vol. 90 (Addison Wesley, Reading, MA 1994) p. 270
45. B.I. Yakobson, C.J. Brabec, J. Bernholc: J. Comput.-Aided Mat. Des. **3**, 173 (1996)
46. J. Fisher: private communication (1997)
47. M.R. Falvo, G.J. Clary, R.M. Taylor II, V. Chi, F.P. Brooks Jr, S. Washburn, R. Superfine: Nature **389**, 582 (1997)
48. B.I. Yakobson, M.P. Campbell, C.J. Brabec, J. Bernholc: Comput. Mat. Sci. **8**, 341–348 (1997)
49. A.J. Stone, D.J. Wales: Chem. Phys. Lett. **128**, 501 (1986)
50. E.L. Briggs, D.J. Sullivan, J. Bernholc: Phys. Rev. B **52**, R5471 (1995); E.L. Briggs, D.J. Sullivan, J. Bernholc: Phys. Rev B **54**, 14362 (1996)
51. B.I. Yakobson: Appl. Phys. Lett. **72**, 918 (1998)